

Addressing stopping failures for small set flip decoding of hypergraph product codes

Lev Stambler¹, Anirudh Krishna², and Michael E. Beverland³

¹*University of Maryland, MD, 20742, USA*

²*Department of Computer Science & Stanford Institute for Theoretical Physics, Stanford, CA, 94305, USA*

³*Microsoft Quantum, Redmond, WA 98052, USA*

November 3, 2023

Abstract

For a quantum error correcting code to be used in practice, it needs to be equipped with an efficient decoding algorithm, which identifies corrections given the observed syndrome of errors. Hypergraph product codes are a promising family of constant-rate quantum LDPC codes that have a linear-time decoding algorithm called Small-Set-Flip (SSF) (Leverrier, Tillich, Zémor FOCS 2015). The algorithm proceeds by iteratively applying small corrections which reduce the syndrome weight. Together, these small corrections can provably correct large errors for sufficiently large codes with sufficiently large (but constant) stabilizer weight. However, this guarantee does not hold for small codes with low stabilizer weight. In this case, SSF can terminate with stopping failures, meaning it encounters an error for which it is unable to identify a small correction. We find that the structure of errors that cause stopping failures have a simple form for sufficiently small qubit failure rates. We propose a new decoding algorithm called the Projection-Along-a-Line (PAL) decoder to supplement SSF after stopping failures. Using SSF + PAL as a combined decoder, we find an order-of-magnitude improvement in the logical error rate.

1 Motivation and main results

Finite-rate quantum low-density parity-check (LDPC) codes are compelling candidates for building quantum memories. The *low density* aspect refers to properties that enable syndrome extraction for these codes to involve each qubit in only a constant number of two-qubit gates, independent of the code size. This limits the spreading of errors which helps ensure that logical errors can be suppressed exponentially as a function of the size of the code. Simultaneously, by virtue of their *finite rate*, the number of physical qubits needed to encode each logical qubit in these codes is independent of the code's size. This offers a considerable benefit over the popular geometrically local code families such as surface codes and color codes which have vanishing rate [1–6].

There is a plethora of constructions of constant-rate quantum LDPC codes, including those based on hyperbolic manifolds [7–9], the hypergraph prod-

uct [10, 11], high-dimensional expanders [12, 13] and algebraic topology [14–16]. Recently, a number of long sought-after ‘good’ quantum codes have been discovered [17, 18], for which both the number of logical qubits and the distance scale linearly with the number of physical qubits. In this work, we focus on the hypergraph product code (HGP) construction, which uses pairs of constant-rate *classical* LDPC codes to build constant-rate *quantum* LDPC codes. While the asymptotic properties of HGP codes fall short of some of the newer families, the HGP construction is arguably the simplest method to build code families with practically reasonable parameters and is the starting point for many of the other constructions.

Decoding algorithms play a crucial role in quantum error correction. These classical algorithms identify a correction from the information output by syndrome extraction. Arguably the most famous example of a decoding algorithm for quantum

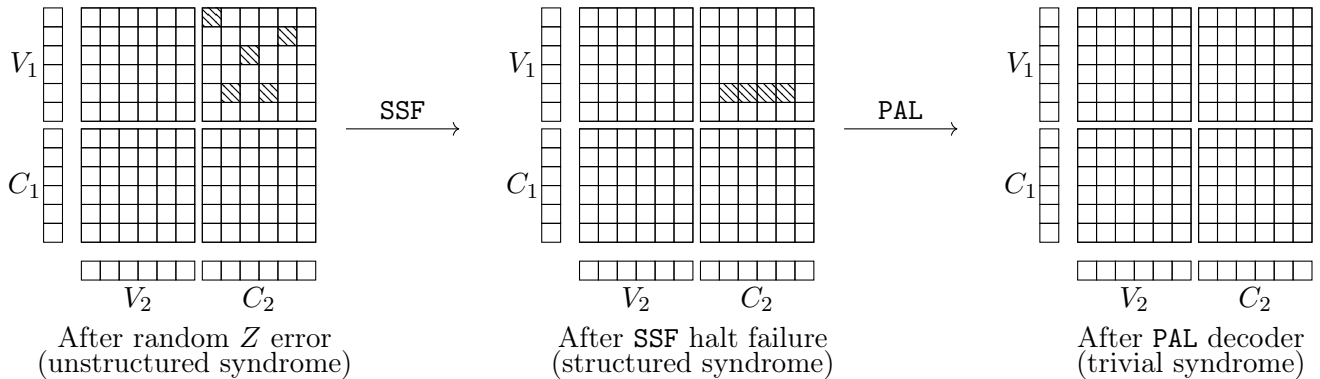


Figure 1: Two-stage decoding of HGP codes. The HGP code has a Tanner graph \mathcal{G} formed from the Cartesian product of the Tanner graphs of two classical codes with bit nodes C_1, C_2 and check nodes V_1, V_2 . Vertices of \mathcal{G} are represented by small squares, with qubits associated with $V_1 \times V_2$ and $C_1 \times C_2$ vertices, while Z and X type stabilizer generators are associated with $C_1 \times V_2$ and $V_1 \times C_2$ vertices respectively. In the first stage, the **SSF** decoder is applied, and if a valid correction is output then decoding is finished. If **SSF** experiences a stopping failure (as in the example depicted), we apply a second decoding stage using the *Projection Along a Line* decoder (**PAL**). Our design of **PAL** exploits the structure of the stopping syndrome which remains after an **SSF** stopping failure, which inherits properties of the classical codes.

LDPC codes is **matching** for surface codes [19, 20], which is based on Edmonds’ graph matching algorithm. This algorithm relies on geometric locality, as do many other decoding algorithms that apply to various geometrically-local codes such as the renormalization-group decoder for topological codes [21] and the projection decoder for color codes [22]. The Union Find decoder [23] notably applies to many codes including non-geometrically local ones [24, 25], but is only known to have a threshold for geometrically-local codes. However, constant-rate quantum LDPC codes are not geometrically local [3–6], necessitating different properties such as graph expansion to form the basis of their decoders.

We focus our attention on Small-Set-Flip (**SSF**), which is a linear-time decoding algorithm for HGP codes introduced by Leverrier, Tillich and Zémor [26]. With adversarial Pauli errors, **SSF** has been proven to efficiently correct errors of weight up to a constant-factor of the code distance [26]. With stochastic Pauli errors with perfect syndrome measurements, which is the noise model we consider in this work, **SSF** has a finite threshold [27]. Moreover, a finite threshold still exists when stochastic

syndrome errors are added (in which case decoding can be performed in a single-shot manner [28]). For these reasons, **SSF** seems very promising for practical applications, motivating further improvements and optimizations to be considered, particularly in parameter regimes of small code sizes and stabilizer weights that are relevant for use in quantum memories.

In this work, we present improvements to the Small-Set-Flip (**SSF**) [26] decoding algorithm for HGP codes. Our primary contribution is to address error configurations for which **SSF** cannot find a correction matching the observed syndrome, which we call a *stopping* failure. The **SSF** algorithm runs iteratively, reducing the syndrome weight in a sequence of rounds by applying partial corrections. Typically when **SSF** terminates in a stopping failure, it has already undergone many rounds and has made partial progress in correcting the error. Moreover, unlike the syndrome of the initial stochastic error introduced by the noise model, we find that the *stopping syndrome* remaining after **SSF** halts tends to be very structured. We exploit this structure to design the Projection Along a Line (**PAL**) decoder that can typ-

ically correct the stopping set output by **SSF** when it results in stopping failures; see Fig. 1.

We note that generalizations of **SSF** [18, 29–31] have been used to design decoders for other families of quantum LDPC codes, including those which have both constant rate and constant relative distance [17, 18]. Consequently, we believe that many of the proposals described in this paper can be generalized to improve decoders for other codes as well.

The structure of the remainder of this paper is as follows. In Section 2, we set notation and review relevant background on error correction, decoders, HGP codes and specify how we perform numerical performance estimates. In Section 3, we analyze stopping failures of the **SSF** decoder, motivate and define the **PAL** decoding algorithm and analyze its performance and time complexity. For instance, we find that for a HGP code with 3600 physical qubits subjected to 1% physical error rate with perfect check measurements, the logical error rate falls from roughly 5×10^{-2} to 4×10^{-4} when moving from the **SSF** decoder to the **SSF** decoder followed by **PAL**. We also discuss a number of approaches to improve the implementation run time of **SSF** in Appendix D.

Related work: Combining **SSF** with other decoding algorithms has been explored before. In [32], **SSF** was applied following Belief Propagation (BP); the combination was referred to as **BP + SSF**.

Connolly *et al.* [33] design a decoding algorithm that also exploits the product structure of HGP codes. Their decoding algorithm reduces the problem of decoding erasure errors on HGP codes to that of decoding erasure errors on a classical code. As a result, their erasure decoding algorithm has complexity $O(N^2)$ in contrast to $O(N^3)$ for generic codes. In Ref. [33], the authors propose one way to apply their approach to the setting of stochastic Pauli noise, namely by using it as a subroutine for the Union Find decoder [23]. However, the Union Find decoder is not known to have a threshold for HGP codes. Our work can be seen as another approach to generalize the work of Connolly *et al.* to the case of stochastic Pauli noise, but in combination with the **SSF** decoder, which is known to have a threshold for HGP codes.

2 Background and notation

In this section we review some important background and fix the notation we use in the rest of the paper.

2.1 Error correction

A classical $[n, k, d]$ error correcting code $\mathcal{C} \subseteq \mathbb{F}_2^n$ is a k -dimensional subspace such that every element has Hamming weight at least d . A code \mathcal{C} can be specified by a parity check matrix $\mathbf{H} \in \mathbb{F}_2^{m \times n}$ —the code is the kernel of \mathbf{H} . Given an error $\mathbf{e} \in \mathbb{F}_2^n$, we let $\boldsymbol{\sigma} = \mathbf{H}\mathbf{e}$ denote its syndrome. A family of codes $\{\mathcal{C}_n\}$ is said to be a low-density parity check (LDPC) family if each row and column of the parity check matrix for each instance has weight upper bounded by a constant independent of n . Equivalently, the code can be specified by its Tanner graph $G = (V \sqcup C, E)$, a bipartite graph where each node $v \in V$ represents a bit and each node $c \in C$ represents a parity check; $(v, c) \in E$ if the bit v is in the support of the check c .

Given a Tanner graph $G = (V \sqcup C, E)$, for two sets $S \subseteq V$ and $T \subseteq C$, we let $E(S, T)$ denote the edges between S and T . For $S \subseteq V$ and $T \subseteq C$, we let $\Gamma(S)$ and $\Gamma(T)$ denote the neighborhood, i.e. the set of nodes adjacent to S and T :

$$\begin{aligned} \Gamma(S) &= \{c \mid E(S, \{c\}) \neq \emptyset\} , \\ \Gamma(T) &= \{v \mid E(\{v\}, T) \neq \emptyset\} . \end{aligned}$$

We let $\tilde{\mathcal{C}}$ represent the $[m, \tilde{k}, \tilde{d}]$ code obtained from G by exchanging the role of the bits and parity checks, which we call the *dual code*.

A *stabilizer group* over N qubits is an Abelian subgroup $\mathcal{S} \subseteq \mathcal{P}_N$ of the N -qubit Pauli group and can be expressed using M independent stabilizer generators

$$\mathcal{S} = \langle S_i : i \in \{1, \dots, M\} \rangle . \quad (1)$$

The stabilizer group defines a *stabilizer code* \mathcal{Q} , which is the space of joint +1-eigenstates of the generators,

$$\mathcal{Q} = \{|\psi\rangle : S|\psi\rangle = |\psi\rangle \ \forall S \in \mathcal{S}\} . \quad (2)$$

The (log-)dimension K of this space is equal to $N - M$ and corresponds to the number of qubits that can be encoded.

The set of *logical operators* \mathcal{L} is the subset of Pauli operators that commute with all the stabilizer generators,

$$\mathcal{L} = \{L : [L, S] = 0 \forall S \in \mathcal{S}\}. \quad (3)$$

The *distance* D of the stabilizer code is the weight of the smallest $L \in \mathcal{L}$ such that L is not in the stabilizer group \mathcal{S} up to a phase.

A family of stabilizer codes $\{\mathcal{Q}_N\}$ is said to be a family of *quantum LDPC codes* if, for all elements \mathcal{Q}_N , each qubit is acted on by at most Δ_q stabilizer generators and each stabilizer generator acts on at most Δ_g qubits. We then say that $\{\mathcal{Q}_N\}$ is an $[[N, K(N), D(N), \Delta_q, \Delta_g]]$ quantum LDPC code family. We say the family has *finite rate* if $K(N) = \Theta(N)$.

The quantum codes we consider in this paper are CSS codes [34, 35], an important class of stabilizer codes for which each stabilizer generator is expressed as either a purely X type or a purely Z type Pauli operator. This then means that the larger decoding task can be broken down into two separate tasks. In this setting, it is convenient to represent the error as a pair of subsets of qubits corresponding to the X and Z support. We focus on correcting only Z -type errors, and precisely the same approach can be used to correct X -type errors. Moreover, both the codes and the noise that we consider are symmetric under the exchange of X and Z , such that the details of any analysis of the correction of Z errors also applies directly to the correction of X errors.

Given a Z error specified by its support $E \subseteq [N]$, the *syndrome* $\sigma(E)$ is a bit string that records the outcomes of a complete set of generators of the stabilizer group. Each bit in $\sigma(E)$ corresponds to a generator $S \in \mathcal{S}$, and is 0 if $Z(E)$ and S commute, and is 1 otherwise.

2.2 Hypergraph product codes

Let $G = (V \cup C, E)$ be a bipartite graph. We assume that G is connected, i.e. there is a path from any vertex to any other vertex in G . We assume G is biregular, i.e. all vertices in V and C have degrees Δ_V and Δ_C respectively.

Let $G_1 = (V_1 \cup C_1, E_1)$ and $G_2 = (V_2 \cup C_2, E_2)$ represent two copies of G . Let $\mathcal{G} = G_1 \times G_2$ denote

the Cartesian product of G with itself. The quantum code is defined with respect to \mathcal{G} as follows:

- The set of physical qubits is associated with the set $V_1 \times V_2 \sqcup C_1 \times C_2$.
- The set of Z type stabilizer generators, denoted \mathcal{Z} , is associated with the set $C_1 \times V_2$. Therefore given $c_1 \in C_1$ and $v_2 \in V_2$, generator (c_1, v_2) is supported on qubits $\Gamma(c_1) \times \{v_2\} \sqcup \{c_1\} \times \Gamma(v_2)$. This set is called the *support* of the generator (c_1, v_2) and denoted $\text{supp}(c_1, v_2)$.
- The set of X type stabilizer generators, denoted \mathcal{X} , is associated with the set $V_1 \times C_2$. Therefore given $v_1 \in V_1$ and $c_2 \in C_2$, generator (v_1, c_2) is supported on qubits $\{v_1\} \times \Gamma(c_2) \sqcup \Gamma(v_1) \times \{c_2\}$.

It is straightforward to see that the stabilizers commute and therefore define a valid quantum code. Consider a Z type stabilizer generator (c_1, v_2) , which has support on qubits $\Gamma(c_1) \times \{v_2\} \sqcup \{c_1\} \times \Gamma(v_2)$. (c_1, v_2) shares support with the set of X type stabilizer generators $\Gamma(c_1) \times \Gamma(v_2)$. This set of parity checks is also called the *local view* of the generator (c_1, v_2) .

Take any one of these X type stabilizer generators, say (v_1, c_2) where $v_1 \in \Gamma(c_1)$ and $c_2 \in \Gamma(v_2)$, and note that this X type stabilizer generator is supported on $\{v_1\} \times \Gamma(c_2) \sqcup \Gamma(v_1) \times \{c_2\}$. (v, c) and (c_1, v_2) therefore share support on precisely two qubits: (v_1, v_2) and (c_1, c_2) and consequently commute. A schematic for the code is presented in Fig. 2.

The parameters of the HGP code are specified by the parameters of the codes \mathcal{C} and $\tilde{\mathcal{C}}$ associated with G . In particular, if \mathcal{C} or $\tilde{\mathcal{C}}$ is constant rate, then so is the resulting quantum code. Furthermore, if G is a graph with bounded degree Δ_V and Δ_C , then the quantum code is an LDPC code that obeys $\Delta_q \leq 2 \max(\Delta_V, \Delta_C)$ and $\Delta_g \leq \Delta_V + \Delta_C$.

We see that HGP codes are CSS codes, and as such we consider only Z type errors. We refer to errors on $V_1 \times V_2$ as VV errors and errors on $C_1 \times C_2$ as CC errors. We refer to X type stabilizer generators as parity checks and Z type stabilizer generators as generators. If a parity check is adjacent to an odd number of (qu)bits with errors, then the parity check is said to be *unsatisfied*; otherwise, it is satisfied.

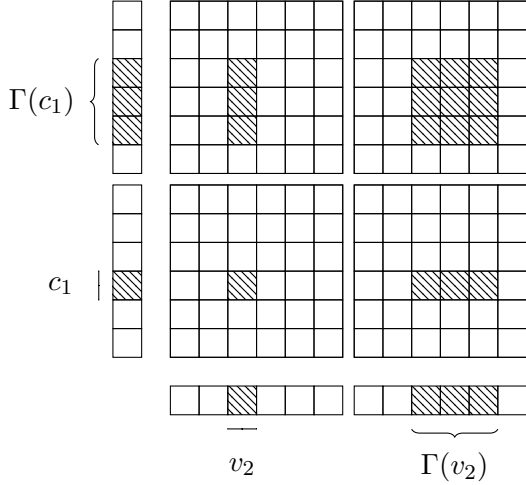
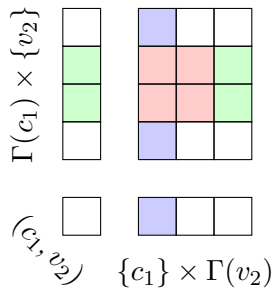


Figure 2: Schematic for the support of a Z type stabilizer generator (c_1, v_2) for $c_1 \in C_1$ and $v_2 \in V_2$.

We explore the structure of a local view of a generator in detail and establish notation as it is central for the decoding algorithm **SSF** (discussed in the next section).

The local view: Let $F \subseteq \text{supp}(c_1, v_2)$ be a set of qubits. Let F_V be the restriction of $F \cap \Gamma(c_1) \times \{v_2\}$ on to the first component and F_C be the restriction of $F \cap \{c_1\} \times \Gamma(v_2)$ on to the second component. In other words, these are the restrictions of F to the VV and CC qubits respectively. We include a figure below to illustrate for a code constructed with a classical graph G such that $\Delta_V = 3$ and $\Delta_C = 4$. The sets F_V and F_C are denoted in green and blue respectively. We let $F_V^c = \Gamma(c_1) \times \{v_2\} \setminus F_V$ and $F_C^c = \{c_1\} \times \Gamma(v_2) \setminus F_C$ denote their complements within the support of (c_1, v_2) .



The *neighborhood* of a set $F \subseteq \text{supp}(c_1, v_2)$, denoted $\Lambda(F)$, is the set of parity checks that is incident to at least one element of F . The neighborhood can be

expressed as the union $\Lambda(F) = F_V \times \Gamma(v_2) \cup \Gamma(c_1) \times F_C$. This corresponds to the union of the colored parity checks in the illustration above.

The *unique neighborhood* of F , denoted $\Lambda^{(u)}(F)$, is the set of parity checks that is incident to one and only one element of F . The unique neighborhood can be expressed as the disjoint union $\Lambda^{(u)}(F) = F_V \times F_C^c \sqcup F_V^c \times F_C$. In the figure above, the unique neighborhood of F is depicted in color corresponding to their unique neighbor—the neighbors of F_V are in green and the neighbors of F_C are in blue. The parity checks in red are also called the multi-neighborhood of F ; we do not introduce separate notation to refer to this set.

2.3 Decoding algorithms

A *decoding algorithm* is a classical algorithm, which, given a syndrome bitstring σ as input, produces a correction consistent with σ . This corresponds to a bitstring $\hat{e} \in \mathbb{F}_2^n$ and a Pauli operator \hat{E} for classical and quantum codes respectively. We refer to these as corrections.

In the quantum case, given an error E , the decoder is passed the syndrome $\sigma(E)$ and either *halts* (it produces no output and declares failure), or outputs a correction \hat{E} with the same syndrome, i.e., $\sigma(\hat{E}) = \sigma(E)$. When the decoder produces an output, it succeeds if the net Pauli applied by both the error and the correction $Z(E)Z(\hat{E}) \in \{\pm i, \pm 1\} \cdot \mathcal{S}$, and fails otherwise.

To recap notation we use throughout this paper:

- e, \hat{e} refers to classical errors interpreted as binary strings of length n .
- E, \hat{E} refers to subsets of $[N]$ corresponding to supports of Pauli operators.
- σ refers to the syndrome of both classical and quantum errors, e.g. $\sigma(e)$ or $\sigma(E)$.
- \oplus denotes the sum of vectors over \mathbb{F}_2 .
- \uplus denotes the symmetric difference of sets.

2.3.1 Small Set Flip

Before describing **SSF** for quantum codes it is informative to briefly review the **FLIP** algorithm for

classical codes which was introduced by Sipser and Spielman [36]. We consider a classical code \mathcal{C} , defined in terms of a (Δ_V, Δ_C) -biregular bipartite Tanner graph $G = (V \cup C, E)$. Let $\mathbf{e} \in \mathbb{F}_2^n$ be an error and let $\boldsymbol{\sigma}$ be the corresponding syndrome. The algorithm is only provided the syndrome $\boldsymbol{\sigma}$ and is initialized with $\hat{\mathbf{e}} = \mathbf{0}$. FLIP is an iterative algorithm such that in each iteration, FLIP tries to find a vertex $v \in V$ to flip, i.e. it maps $\hat{\mathbf{e}}_v \mapsto \hat{\mathbf{e}}_v \oplus 1$, such that the syndrome weight decreases. The algorithm terminates when no such vertex v exists. For the FLIP algorithm to succeed, when the algorithm terminates $\mathbf{e} = \hat{\mathbf{e}}$. There are two modes of failure. First, it can find a valid correction $\hat{\mathbf{e}}$ such that $\hat{\mathbf{e}} + \mathbf{e}$ is a logical error, which we call an error correction failure. Second, it can terminate with a non-zero syndrome, a failure mode that we call a *halt failure*.

To guarantee FLIP succeeds, we require that the bipartite graph G that defines the code \mathcal{C} corresponds to an expander, i.e. for all $S \subseteq V$,

$$|S| \leq \alpha n \implies |\Gamma(S)| \geq (1 - \epsilon)\Delta_V |S|, \quad (4)$$

where $0 < \alpha < 1$ and $0 < \epsilon < 1/4$ are parameters of G . The algorithm can correct errors \mathbf{e} whose weight is a constant fraction of the code distance.

Small Set Flip (SSF) is an iterative decoding algorithm for quantum codes that generalizes FLIP. In the iteration indexed by i , it applies an update to the correction and correspondingly updates the syndrome to $\boldsymbol{\sigma}^{(i)}$. When it can no longer update the syndrome, it terminates.

For any $F \subseteq [N]$, we define the **score** function as

$$\text{score}(F) = \left\{ \frac{|\boldsymbol{\sigma}^{(i)}| - |\boldsymbol{\sigma}^{(i)} \oplus \boldsymbol{\sigma}(F)|}{|F|} \right\}, \quad (5)$$

where \oplus denotes the sum mod 2. In the special case that F is empty, we define $\text{score}(F) = 0$.

The score of a set F captures how good a partial Z type correction F is. The numerator of the score function corresponds to the change in the syndrome weight that would be caused by flipping F . The denominator, on the other hand, assigns a higher score to F if its weight is lower. In particular, if we have two candidates F and F' that cause the same change in syndrome but obey $|F| < |F'|$, then $\text{score}(F) > \text{score}(F')$.

Let \mathcal{F} denote the union of all subsets F contained in the support of any Z type generator:

$$\mathcal{F} = \{F : F \subseteq \text{supp}(S), S \in \mathcal{Z}\}. \quad (6)$$

SSF, as specified in Algorithm 1, is an iterative algorithm where in each iteration, the *score* is evaluated for each element $F \in \mathcal{F}$, and then a set with the maximum score is applied as a partial correction (if positive), which reduces the syndrome weight.

Algorithm 1 SSF($\boldsymbol{\sigma}(E)$) (Informal)

Input: A syndrome $\boldsymbol{\sigma}(E) \in \mathbb{F}_2^M$.
Output: Correction \hat{E}

- 1: $i \leftarrow 0$
- 2: $\boldsymbol{\sigma}^{(0)} \leftarrow \boldsymbol{\sigma}(E)$
- 3: $\hat{E} \leftarrow \emptyset$
- 4: $F_0 \leftarrow \arg \max \text{score}(F)$ over $F \in \mathcal{F}$
- 5: **while** $\text{score}(F_i) > 0$ **do**
- 6: $\hat{E} \leftarrow \hat{E} \uplus F_i$
- 7: $\boldsymbol{\sigma}^{(i+1)} \leftarrow \boldsymbol{\sigma}^{(i)} \oplus \boldsymbol{\sigma}(F_i)$
- 8: $i \leftarrow i + 1$
- 9: $F_i \leftarrow \arg \max \text{score}(F)$ over $F \in \mathcal{F}$
- 10: **return** \hat{E} .

It may appear at first that this algorithm formally has run time $O(N \log N)$ rather than $O(N)$ since the list of scores needs to be stored and updated in order to pick out the maximum at each round, and comparison sorting requires time $\Omega(N \log N)$. However, there is a finite set of allowed scores since the size of each element in \mathcal{F} is limited by the size of the largest stabilizer generator which also implies a finite set of allowed syndrome differences in each iteration. Sorting a set of N elements which only take values in a finite range only requires time $O(N)$ using **counting sort** [37]. In practice, this makes little difference in the run time of instances in the regimes we consider in this paper and we use a standard comparison-based sorting algorithm in our implementations. Note that we provide a more formal version of Algorithm 1, namely Algorithm 6 in Appendix D, which includes further details of the data structures used.

While SSF is a linear-time algorithm, the dependence of the time complexity on the degree of the quantum LDPC code scales poorly. For a specific generator $S \in \mathcal{Z}$, evaluating the scores takes

$\Theta(2^{|\text{supp}(S)|})$ time since that generator contributes $2^{|\text{supp}(S)|}$ elements to \mathcal{F} . For a fixed family of LDPC codes, this quantity is a constant as Δ_V and Δ_C are constants, but it can be large.

There are two modes of failure for the **SSF** decoding algorithm. First, it can find a valid correction \widehat{E} such that $Z(E) \cdot Z(\widehat{E})$ is a logical error, which we call an error correction failure. Second, it can terminate with a non-zero syndrome, a failure mode that we call a halt failure. We count both as logical failures. For a fixed code \mathcal{Q} in the code family, an error E on which **SSF** cannot complete even one iteration is called a stopping set. Stopping sets have been explored in the context of other iterative decoding algorithms and other quantum codes (e.g. [38]). When **SSF** terminates with a halt failure, the stopping sets correspond to stopping sets of **SSF**; we refer to the corresponding syndromes as stopping syndromes.

2.3.2 Belief Propagation and Ordered Statistics Decoding

Here we provide high-level overviews of a Belief Propagation (BP) decoder and an Ordered Statistics Decoder (OSD) for classical codes. We use these decoders as subroutines for the **PAL** decoder which we introduce in Section 3. For simulations in this paper, we use the open-source implementation of BP and OSD in the software package by Joschka Roffe [39] with specific parameter settings as described in Appendix B.

The term ‘BP decoder’ is really an umbrella term for a class of decoding algorithms on Tanner graphs, which calculate the marginal probability of an error on each bit given the observed syndrome. Since the marginal probability of an error on a given bit depends on the probability of errors on other bits, information is iteratively passed between neighbors in the graph, to approximate the most probable distribution over bits. This process ideally converges to a consistent probability distribution that can be used to infer a correction. In this paper, we use the implementation from [39] which is a min-sum implementation of BP, and henceforth refer to that implementation simply as BP.

If the physical failure probability of each bit is decreased, we expect the logical failure probabil-

ity to decrease as well. However, BP can instead run into an ‘error floor’—where the logical failure rate plateaus rather than decreasing with further iterations. This can be caused by feedback loops in BP due to the existence of cycles in the Tanner graph [40].

The Ordered Statistics Decoder [41] is a classical decoder by Fossosier and Lin, which when generalized to the quantum setting can overcome the problem of feedback loops that are experienced by BP [42] and can perform well in practice for quantum codes [43]. Here we focus on OSD as a classical decoder however.

The OSD algorithm involves separating the n bits of the code into two sets: a set T of $n - m$ bits which we are confident have *not* been flipped, and a set S of m bits which may or may not have been flipped. The set S the code’s $n \times m$ parity check matrix H restricted to columns in S is invertible (i.e. the m columns are linearly independent). First, we run BP and the columns of H are sorted (say, from left to right) according to the confidence with which we believe they are flipped. This results in a partition of H (up to column permutations) of the following form

$$H = (H_S | H_T) ,$$

where the columns of H_S are linearly independent, i.e. H_S is invertible and all the bits in S correspond to bits that are flipped. In this ordering, we more strongly believe that the bit indexed by the j^{th} column of H has been flipped than the bit indexed by the $(j + 1)^{\text{th}}$ column of H . A solution \widehat{e} to the equation $H\mathbf{e} = \boldsymbol{\sigma}$ can be expressed as $\widehat{e} = (\widehat{e}_S | \widehat{e}_T)$. As H_S is invertible, for every choice of \widehat{e}_T , there exists a unique choice of \widehat{e}_S such that $H\widehat{e} = \boldsymbol{\sigma}$.

As the columns of H_S are linearly independent, we can find a solution of the form $\widehat{e}^{(0)} = (\widehat{e}_S^{(0)} | \mathbf{0})$. However, this solution need not be the most likely solution—there may exist a correction $\widehat{e}' = (\widehat{e}'_S | \widehat{e}'_T)$ with lower weight than $\widehat{e}^{(0)}$. To find the most likely solution, one iterates through every possible choice of \widehat{e}_T . For a constant rate code, this algorithm requires exponential time as \widehat{e}_T is supported on $n - m = \Theta(n)$ bits. However, there exist efficient approximations that only use low weight strings \widehat{e}_T . We use the variant BP-OSD-CS by Roffe *et al.* [43] that we refer to simply as BP-OSD. In this variant,

all weight 2 solutions in T are considered.

This algorithm runs in $O(n^3)$ time for codes of size n , where the dominant cost is Gaussian elimination for the matrix inversion step.

2.4 Numerical tests of decoder run time and error correction performance

The HGP codes which we use for our examples are specified as follows. Bipartite graphs with bounded degree corresponding to classical codes are constructed using the Progressive Edge Growth (PEG) algorithm [44]. The classical codes themselves correspond to $(3, 4)$ -biregular bipartite graphs; this results in quantum codes with $\Delta_q \leq 8$, $\Delta_g \leq 7$.

In this work we assume that X and Z errors are decoded independently, and since the codes are symmetric under the exchange of X and Z we consider only Z errors. We assume that each qubit independently undergoes a Z error with probability p_{phys} , resulting in a Z type error specified by a bitstring E , which has an X -type syndrome $\sigma(E)$, which we assume is extracted perfectly. We then run the implementation of the decoder on this syndrome, which either produces a proposed correction \hat{E} , or experiences a halting failure. If the combined effect of the proposed correction and the error, namely $Z(E) \cdot Z(\hat{E})$, is a Z stabilizer, the decoder succeeds; otherwise, we say that a *logical* failure has occurred.

We adhere to the following rules in order to take data for numerical comparisons:

1. We present the average costs over all samples.
2. We take sufficiently many samples such that the statistical uncertainty of failure probabilities appear only at the second significant figure.

3 Decoding after SSF halt failures

The SSF decoder has proven performance guarantees for HGP codes with sufficiently large input graphs with sufficiently large degree [26]¹. However, for practical purposes we are more interested in HGP

¹Formally, these guarantees are expressed in terms of a property called *graph expansion*; SSF is guaranteed to converge for graphs with sufficient expansion.

codes built from small input graphs with more modest degree. In this regime SSF often does not find a correction and instead terminates with a stopping failure; see Table 1.

In the standard version of SSF presented in Section 2, stopping failures are treated as bona fide failures. Before it stops, however, SSF can undergo many rounds resulting in a partial correction that significantly reduces the syndrome weight compared with that of the initial error.

In Section 3.1 we show that the stopping syndromes tend to exhibit a specific structure. In Section 3.2 we propose a new decoding algorithm that can often exploit this structure to correct the stopping set. We call this the Projection-Along-a-Line (PAL) decoder. In Section 3.3 we analyze the performance of the two-step decoder formed by applying SSF followed by PAL, finding order-of-magnitude improvements over SSF alone in regimes of interest.

3.1 Understanding stopping failures

Here we seek to understand syndrome patterns that cause the SSF decoder to halt for HGP codes.

As explained in Section 2.3.1, SSF is an iterative algorithm which monotonically reduces the syndrome weight over a sequence of rounds by applying a partial correction in each round until either the syndrome is completely removed or a stopping syndrome is reached. Stopping syndromes have the property that none of the potential corrections offered by SSF can reduce their syndrome weight. As fixed points of the SSF algorithm, stopping syndromes are much more structured than syndromes corresponding to random errors applied by the noise model. Furthermore, many different initial syndromes generated by random errors can flow to the same stopping syndrome under SSF.

To understand the structure of stopping syndromes it is informative to consider the structure of the HGP codes that we reviewed in Section 2.2. For concreteness, consider an HGP code associated with a graph $\mathcal{G} = G_1 \times G_2$, formed from two copies (G_1 and G_2) of the bipartite graph $G = (V \cup C, E)$, which we assume is (Δ_V, Δ_C) biregular. Let \mathcal{C} ($\hat{\mathcal{C}}$) be the code obtained by associating V (C) with the bits and C (V) with the parity checks.

class of stopping sets from the contrived starting point of a line-like initial syndrome, our numerical studies show that in fact a very large fraction of stopping syndromes are of this type given stochastic initial errors (which rarely have line-like initial syndromes). This can be seen in Table 1 which shows the frequency of the minimal number of lines needed to cover the support of the stopping syndromes observed for **SSF** for a variety of HGP code sizes and error rates.

We end this subsection with some (non-rigorous) intuition for why one might expect stopping syndromes to be line-like for unstructured random errors when the error rates are sufficiently low. When error rates are low, the errors are likely to be isolated and far from each other with respect to the graph \mathcal{G} , which will produce a syndrome which forms small clusters, with clusters being far apart with respect to the graph \mathcal{G} . Clusters of syndromes that are far apart in the graph \mathcal{G} are handled independently by **SSF**, which only applies corrections within the support of generators, and these clusters will tend to shrink as the algorithm proceeds, many of them disappearing. At some point, the syndrome will be very sparse, and will most likely lie on a small number of lines just by virtue of having low density, most of these line-like syndromes can be expected to be uncoupled as far as **SSF** is concerned because they are far apart in the graph \mathcal{G} . If the syndrome restricted to a line is uncoupled from the rest of the system, then it will be treated by **SSF** as if it were being handled by **FLIP** on the classical code as discussed above. Eventually only those clusters which are line-like and stopping syndromes for the classical codes remain. As we expect these classical stopping syndromes to be rare, probably none will arise and **SSF** will simply finish by producing a valid correction. With some small chance, one or more classical stopping syndromes will have been produced (causing a stop failure for **SSF**). If the qubit failure rate is increased beyond this low error rate regime, errors form larger clusters that are not very well separated on the graph. The stopping sets begin to look more complex as errors on multiple lines begin to interact. The structure of the stopping syndromes ceases to have an easily discernible form.

3.2 PAL decoding algorithm

Our algorithm proceeds iteratively. First, we express the syndrome as contributions from different lines and these are sorted into **hor** and **vert** for horizontal and vertical lines respectively. Points are counted as both horizontal and vertical lines. For each line $\ell \in \text{hor} \cup \text{vert}$, we obtain a correction F_ℓ . We then apply the correction with the maximum score, i.e. the correction F_ℓ that maximizes the score defined in Eq. 5

$$\text{score}(F_\ell) = \frac{|\sigma| - |\sigma \oplus \sigma(F_\ell)|}{|F_\ell|}.$$

Algorithm 2 presented below describes how we classify syndromes into lines. In our implementa-

Algorithm 2 GetLines(σ)

Input: Syndrome $\sigma \in \mathbb{F}_2^{V_1 \times C_2}$,

Output: hor, vert.

- 1: **hor, vert** $\leftarrow \emptyset$ will be the set of horizontal and vertical lines.
 - 2: **for** $v \in V$ **do**
 - 3: $\text{hor} \leftarrow \text{hor} \cup (\{v\} \times C \cap \sigma)$
 - 4: **for** $c \in C$ **do**
 - 5: $\text{vert} \leftarrow \text{vert} \cup (V \times \{c\} \cap \sigma)$
 - 6: **return** hor, vert
-

tion of Algorithm 2, we use a dictionary to decrease the run time from $O(|\sigma|^2)$, as specified in the pseudocode, to $O(|\sigma|)$.

GetLines accepts as input the syndrome $\sigma \in \mathbb{F}_2^{V_1 \times C_2}$. For each $v_1 \in V_1$, it scans through σ , and if it finds any unsatisfied parity checks supported on the subset $\{v_1\} \times C_2$, then it classifies this as a *horizontal* line. It repeats a similar process for every $c_2 \in C_2$ and scans for unsatisfied parity checks supported on $V_1 \times \{c_2\}$ ².

The **PAL** algorithm, described in Algorithm 3, is an iterative decoding algorithm that takes the classification into lines as input. It decodes each set in $\text{hor} \cup \text{vert}$ separately using **BP-OSD** as stated in Line 9. These lines are interpreted as syndromes corresponding to errors on classical codes; an element of **hor** of the form $\{v_1\} \times C_2$ will only return a correction within $\{v_1\} \times V_2$. Similarly, an element in

²We find **hor** and **vert** may contain elements in common corresponding to syndromes that are isolated points.

Algorithm 3 PAL(σ)

Input: Syndrome $\sigma \in \mathbb{F}_2^{V_1 \times C_2}$,
Output: Correction \hat{E}

- 1: $i \leftarrow 0$
- 2: $\hat{E} \leftarrow \emptyset$.
- 3: $\text{hor}, \text{vert} \leftarrow \text{GetLines}(\sigma)$
- 4: $\text{lines} \leftarrow |\text{hor}| + |\text{vert}|$.
- 5: **while** $\text{lines} > 0$ and $i < \mathcal{I}$ **do**
- 6: $i \leftarrow i + 1$
- 7: $F_i \leftarrow 0$
- 8: **for** $\sigma_j \in \text{hor} \cup \text{vert}$ **do**
- 9: $F_j \leftarrow \text{BP-OSD}(\sigma_j)$.
- 10: **if** $\text{score}(F_j) > \text{score}(F_i)$ **then**
- 11: $F_i \leftarrow F_j$
- 12: $\hat{E} \leftarrow \hat{E} \uplus F_i$
- 13: $\sigma \leftarrow \sigma \oplus \sigma(F_i)$
- 14: $\text{hor}, \text{vert} \leftarrow \text{GetLines}(\sigma)$
- 15: $\text{lines} \leftarrow |\text{hor}| + |\text{vert}|$.
- 16: **return** \hat{E} .

vert of the form $V_1 \times \{c_2\}$ will only return a correction within $C_1 \times \{c_2\}$. To be precise, we define two versions of BP-OSD in our implementation—one used for `hor` and the other used for `vert`. Line 9 does not include this complexity for conceptual clarity and ease of presentation. We highlight that any decoding algorithm for classical codes can be used here in principle. BP-OSD has the best performance among the heuristics we tried.

In each iteration, we flip the line whose correction has the largest score. This continues until the syndrome is the 0 string or until the total number of iterations is \mathcal{I} . As the physical error rate increases, the number of required iterations grows. In our simulations, we set $\mathcal{I} = 20$ as an upper bound.

The complete decoding algorithm is presented below in Algorithm 4.

To run BP-OSD on each classical code, we need to know how to initialize log-likelihood ratios (LLRs) for each line. Setting the initial LLRs for BP-OSD is not trivial. Indeed, for a fixed qubit failure rate p_{phys} , SSF may manage to correct at least some of the initial errors before it terminates. Therefore, the distribution of errors along a line can be very

Algorithm 4 Decode(σ)

Input: Syndrome $\sigma \in \mathbb{F}_2^{V_1 \times C_2}$
Output: Correction \hat{E} if algorithm converges and FAIL otherwise.

- 1: $\hat{E}_{\text{SSF}} \leftarrow \text{SSF}(\sigma)$
- 2: $\hat{E}_{\text{PAL}} \leftarrow \text{PAL}(\sigma(\hat{E}_{\text{SSF}}))$
- 3: **if** $\sigma(\hat{E}_{\text{SSF}} \uplus \hat{E}_{\text{PAL}}) \oplus \sigma$ is zero **then**
- 4: **return** $\hat{E} \leftarrow \hat{E}_{\text{SSF}} \uplus \hat{E}_{\text{PAL}}$
- 5: **else**
- 6: **return** FAIL (halt).

different from the physical failure rate p_{phys} . For example, errors may be “concentrated” along a specific line, i.e. while the total number of errors in the HGP code decreases, some lines may end up with more errors than they began with. In Appendix B, we include the details required to initialize and run BP-OSD along each line.

One could consider a further optimized version where we could infer the physical bit error rates q_V and q_C as a function of both p_{phys} but also as a function of the number of syndromes along that line. Instead, we take an average over all possible lines.

Time complexity of SSF + PAL: The time complexity of the SSF decoder is $O(N)$. The complexity of the PAL decoder depends on the number of lines and on the complexity of BP-OSD. The latter is straightforward – it is $O(N^{3/2})$ per line as BP-OSD runs in $O(n^3)$ time for codes of block length n and each line is a code of length $O(\sqrt{N})$. However, as the number of lines is itself a random variable, we can only heuristically estimate the complexity of SSF + PAL. Algorithm 2 takes time $O(N)$. The number of lines after each round of PAL does not increase. To see why, note that applying any correction along a line does not increase the number of lines.

With this observation, suppose there are L lines. Recall that PAL is permitted to run for a maximum number of iterations \mathcal{I} . Therefore, the total complexity of BP-OSD is at most $O(\mathcal{I} \cdot L \cdot N^{3/2})$.

3.3 Results of numerical simulations

The results of our simulations are presented in Fig. 4. For low qubit failure rates, PAL improves the decoding performance by at least an order-of-magnitude. For instance, consider the HGP code obtained as a product of (3, 4) biregular graphs. At 1% physical error rates, the logical error probability for the code with 3600 physical qubits falls from roughly 5×10^{-2} to 4×10^{-4} . The multiple by which the logical error rate decreases improves as we decrease the qubit failure rate.

4 Conclusions and future work

We have studied failures for Small-Set-Flip (SSF) on hypergraph product codes. We focused on stopping failures, instances where SSF terminates without entirely correcting the error. The error when SSF terminates was called the stopping set and the corresponding syndrome the stopping syndrome. We found that the stopping syndromes supported on lines in the hypergraph product code. A line corresponds to a subgraph of the hypergraph product code of the form $\{v_1\} \times C_2$ for $v_1 \in V_1$ or $V_1 \times \{c_2\}$ for $c_2 \in C_2$. As these lines correspond to classical codes \mathcal{C} and $\tilde{\mathcal{C}}$, this allowed us to reduce the problem of decoding a quantum code to decoding a classical code. To this end, we propose using the Projection-Along-a-Line decoder (PAL) after SSF.

The algorithm PAL is itself an iterative algorithm; in each iteration, it identifies corrections along a line. As the stopping syndrome can be supported on lines that share parity checks, the corrections along different lines are not independent. We use an appropriately defined score function to pick one line and the corresponding correction. Intuitively, this corresponded to the correction that reduces the syndrome the most with least number of flips.

While PAL allows for any classical decoding algorithm to be used as a subroutine, we have used BP-OSD. We found that for error rates of 1% or lower, the logical failure rate can improve by an order-of-magnitude.

One can consider the use of PAL as a post-decoder for other decoders. In Appendix C we compare the performance of the BP + SSF decoder with

BP + SSF + PAL with HGP codes built from (3,4)-biregular graphs. In this setting, we find that the improvements due to PAL are negligible, since the ratio of failures which are stop type for BP + SSF is small in this case. It would be interesting to explore larger degree HGP codes and other decoders to find more suitable applications of PAL.

In Appendix D, we explain our implementation of SSF in detail, and include some techniques to modestly reduce the time complexity for quantum codes constructed via the product of (3, 4) biregular graphs.

5 Acknowledgements

We thank Anthony Leverrier & Nicolas Delfosse for comments. LS would like to thank Patrick Hayden and the Stanford Institute for Theoretical Physics for hosting his visit while this research was undertaken.

AK acknowledges support from the Bloch Postdoctoral Fellowship at Stanford University and NSF grant CCF-1844628.

References

- [1] A.A. Kovalev and L.P. Pryadko. Improved quantum hypergraph-product LDPC codes. In *Information Theory Proceedings (ISIT), 2012 IEEE International Symposium on*, pages 348–352. IEEE, 2012.
- [2] D. Gottesman. Fault-tolerant quantum computation with constant overhead. *Quantum Information & Computation*, 14(15-16):1338–1372, 2014.
- [3] S. Bravyi, D. Poulin, and B. Terhal. Trade-offs for reliable quantum information storage in 2D systems. *Physical Review Letters*, 104(5):050503, 2010.
- [4] N. Baspin and A. Krishna. Connectivity constrains quantum codes. *Quantum*, 6:711, 2022.
- [5] N. Baspin and A. Krishna. Quantifying non-locality: How outperforming local quantum codes is expensive. *Physical Review Letters*, 129(5):050505, 2022.

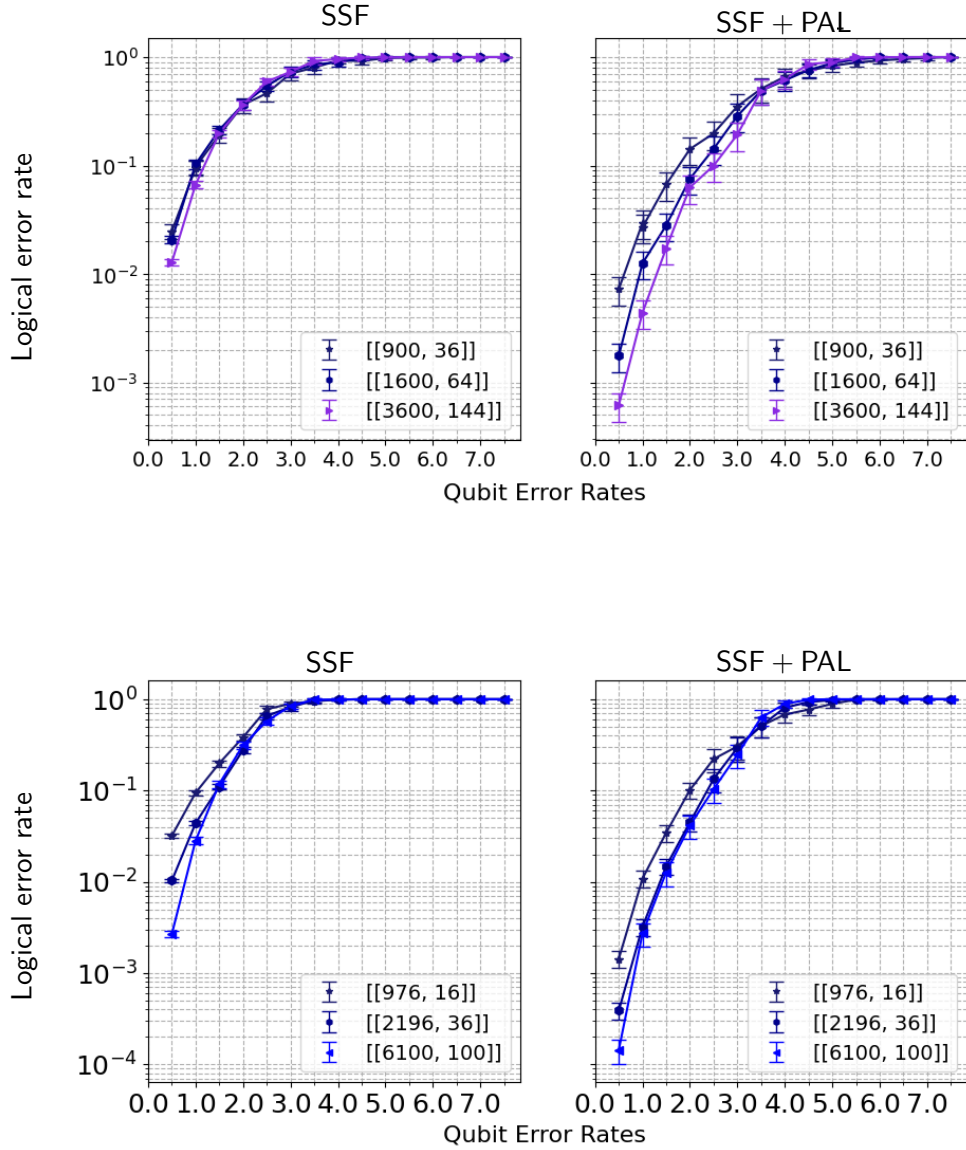


Figure 4: Comparing the change in logical error probability before and after the post-processing algorithm PAL for the hypergraph product code constructed from $(3, 4)$ -biregular bipartite graphs (upper panels) and $(5, 6)$ -biregular bipartite graphs (lower panels). This results in a family of quantum codes with $\Delta_q = 8, \Delta_g = 7$ (upper panels) and $\Delta_q = 12, \Delta_g = 11$ (lower panels). The error bars represent the 95% confidence intervals, i.e. ≈ 1.96 standard deviations. We note that there is not a very smooth improvement of the curves for successive codes for the $(5, 6)$ case. We believe this is due to the random procedure used to generate the classical codes.

- [6] N. Baspin, V. Guruswami, A. Krishna, and R. Li. Improved rate-distance trade-offs for quantum codes with restricted connectivity. *arXiv preprint arXiv:2307.03283*, 2023.
- [7] M.H. Freedman, D.A. Meyer, and F. Luo. Z2-systolic freedom and quantum codes. In *Mathematics of quantum computation*, pages 303–338. Chapman and Hall/CRC, 2002.
- [8] L. Guth and A. Lubotzky. Quantum error correcting codes and 4-dimensional arithmetic hyperbolic manifolds. *Journal of Mathematical Physics*, 55(8):082202, 2014.
- [9] V. Londe and A. Leverrier. Golden codes: quantum LDPC codes built from regular tessellations of hyperbolic 4-manifolds. *Quantum Information & Computation*, 19(5-6):361–391, 2019.
- [10] J.P. Tillich and G. Zémor. Quantum LDPC codes with positive rate and minimum distance proportional to the square root of the block-length. *IEEE Transactions on Information Theory*, 60(2):1193–1202, 2014.
- [11] W. Zeng and L.P. Pryadko. Higher-dimensional quantum hypergraph-product codes with finite rates. *Physical review letters*, 122(23):230501, 2019.
- [12] S. Evra, T. Kaufman, and G. Zémor. Decodable quantum LDPC codes beyond the square root distance barrier using high dimensional expanders. In *2020 IEEE 61st Annual Symposium on Foundations of Computer Science (FOCS)*, pages 218–227. IEEE, 2020.
- [13] T. Kaufman and R.J. Tessler. New cosystolic expanders from tensors imply explicit quantum LDPC codes with $\omega(\sqrt{n} \log^k n)$ distance. In *Proceedings of the 53rd Annual ACM SIGACT Symposium on Theory of Computing*, pages 1317–1329, 2021.
- [14] M.B. Hastings, J. Haah, and R. O’Donnell. Fiber bundle codes: breaking the $n^{1/2} \text{poly} \log(n)$ barrier for quantum LDPC codes. In *Proceedings of the 53rd Annual ACM SIGACT Symposium on Theory of Computing*, pages 1276–1288, 2021.
- [15] N.P. Breuckmann and J.N. Eberhardt. Balanced product quantum codes. *IEEE Transactions on Information Theory*, 67(10):6653–6674, 2021.
- [16] T.C. Lin and M.H. Hsieh. Good quantum LDPC codes with linear time decoder from lossless expanders. *arXiv preprint arXiv:2203.03581*, 2022.
- [17] P. Panteleev and G. Kalachev. Asymptotically good quantum and locally testable classical LDPC codes. In *Proceedings of the 54th Annual ACM SIGACT Symposium on Theory of Computing*, pages 375–388, 2022.
- [18] A. Leverrier and G. Zémor. Quantum tanner codes. *arXiv preprint arXiv:2202.13641*, 2022.
- [19] A.Y. Kitaev. Quantum computations: algorithms and error correction. *Russian Mathematical Surveys*, 52(6):1191–1249, 1997.
- [20] S.B. Bravyi and A.Y. Kitaev. Quantum codes on a lattice with boundary. *arXiv preprint quant-ph/9811052*, 1998.
- [21] G. Duclos-Cianci and D. Poulin. Fast decoders for topological quantum codes. *Physical Review Letters*, 104(5):050504, 2010.
- [22] N. Delfosse. Decoding color codes by projection onto surface codes. *Physical Review A*, 89(1):012317, 2014.
- [23] N. Delfosse and N.H. Nickerson. Almost-linear time decoding algorithm for topological codes. *Quantum*, 5:595, 2021.
- [24] N. Delfosse and M.B. Hastings. Union-find decoders for homological product codes. *Quantum*, 5:406, 2021.
- [25] N. Delfosse, V. Londe, and M.E. Beverland. Toward a union-find decoder for quantum LDPC codes. *IEEE Transactions on Information Theory*, 68(5):3187–3199, 2022.
- [26] A. Leverrier, J.P. Tillich, and G. Zémor. Quantum expander codes. In *Foundations of Computer Science (FOCS), 2015 IEEE 56th Annual Symposium on*, pages 810–824. IEEE, 2015.

- [27] O. Fawzi, A. Grospellier, and A. Leverrier. Efficient decoding of random errors for quantum expander codes. In *Proceedings of the 50th Annual ACM SIGACT Symposium on Theory of Computing*, pages 521–534, 2018.
- [28] O. Fawzi, A. Grospellier, and A. Leverrier. Constant overhead quantum fault-tolerance with quantum expander codes. In *2018 IEEE 59th Annual Symposium on Foundations of Computer Science (FOCS)*, pages 743–754. IEEE, 2018.
- [29] A. Leverrier and G. Zémor. Efficient decoding up to a constant fraction of the code length for asymptotically good quantum codes. *arXiv preprint arXiv:2206.07571*, 2022.
- [30] A. Leverrier and G. Zémor. A parallel decoder for good quantum LDPC codes. *arXiv preprint arXiv:2208.05537*, 2022.
- [31] S. Gu, C.A. Pattison, and E. Tang. An efficient decoder for a linear distance quantum LDPC code. *arXiv preprint arXiv:2206.06557*, 2022.
- [32] A. Grospellier, L. Grouès, A. Krishna, and A. Leverrier. Combining hard and soft decoders for hypergraph product codes. *Quantum*, 5:432, Apr. 2021.
- [33] N. Connolly, V. Londe, A. Leverrier, and N. Delfosse. Fast erasure decoder for a class of quantum LDPC codes. *arXiv preprint arXiv:2208.01002*, 2022.
- [34] A.R. Calderbank and P.W. Shor. Good quantum error-correcting codes exist. *Physical Review A*, 54(2):1098, 1996.
- [35] A. Steane. Multiple-particle interference and quantum error correction. *Proceedings of the Royal Society A*, 452(1954):2551–2577, 1996.
- [36] M. Sipser and D.A. Spielman. Expander codes. In *Foundations of Computer Science, 1994 Proceedings., 35th Annual Symposium on*, pages 566–576. IEEE, 1994.
- [37] T.H. Cormen, C.E. Leiserson, R.L. Rivest, and C. Stein. *Introduction to Algorithms*. The MIT Press, 2nd edition, 2001.
- [38] N. Raveendran. *Trapping Sets of Iterative Decoders for Quantum and Classical Low-Density Parity-Check Codes*. PhD thesis, The University of Arizona, 2021.
- [39] J. Roffe, D.R. White, S. Burton, and E. Campbell. Decoding across the quantum low-density parity-check code landscape. *Physical Review Research*, 2(4), Dec 2020.
- [40] D. Poulin and Y. Chung. On the iterative decoding of sparse quantum codes. *arXiv preprint arXiv:0801.1241*, 2008.
- [41] M.P. Fossorier and S. Lin. Soft-decision decoding of linear block codes based on ordered statistics. *IEEE Transactions on Information Theory*, 41(5):1379–1396, 1995.
- [42] P. Panteleev and G. Kalachev. Degenerate quantum LDPC codes with good finite length performance. *Quantum*, 5:585, 2021.
- [43] J. Roffe, D.R. White, S. Burton, and E. Campbell. Decoding across the quantum low-density parity-check code landscape. *Physical Review Research*, 2(4):043423, 2020.
- [44] X.Y. Hu, E. Eleftheriou, and D.M. Arnold. Progressive edge-growth tanner graphs. In *GLOBECOM'01. IEEE Global Telecommunications Conference (Cat. No. 01CH37270)*, volume 2, pages 995–1001. IEEE, 2001.
- [45] A. Grospellier and A. Krishna. Numerical study of hypergraph product codes. *arXiv preprint arXiv:1810.03681*, 2018.
- [46] R.W. Doran. The gray code. Technical report, Department of Computer Science, The University of Auckland, New Zealand, 2007.

A Proof of Lemma

[Proof of Lemma 1]

In this section we prove Lemma 1, which concerns the support of a correction applied by SSF when the syndrome is line-like.

First, we rule out trivial cases—the vast majority of Z stabilizer generators will not participate.

Flipping qubits that are not themselves supported on the line can only *increase* the syndrome weight. Even though it is a trivial observation, we formally state this in the following claim.

Claim 2. *If F is in the support of a Z stabilizer generator whose local view does not contain UNSAT, then the weight of the syndrome can only increase by flipping F .*

Consequently, SSF will only apply corrections from within stabilizer generators that are adjacent to the line, i.e. using stabilizer generators that contain within their support qubits in the line. This corresponds to Z stabilizer generators of the form $\Gamma(v_1) \times V_2$. With this observation, we proceed to study only stabilizer generators that contain UNSAT in the local view.

Next, we ask how the weight of the syndrome changes when a set of qubits F is flipped. Consider sets F within the support of (c_1, v_2) for $c_1 \in \Gamma(v_1)$. Let $F \subseteq \text{supp}(c_1, v_2)$ and let $F_V = F \cap V_1 \times V_2$ and $F_C = F \cap C_1 \times C_2$ be the support of the flip on VV and CC qubits respectively. If we flip the set F , parity checks that are adjacent to a single qubit in F will be affected whereas parity checks that are adjacent to two qubits in F will remain unaffected. Recall that the set of parity checks adjacent to a single qubit of F is called the unique neighborhood of F and is denoted $\Lambda^{(u)}(F)$.

Observation: If any unsatisfied parity checks overlap the unique neighborhood, they will be flipped; these are supported on $\Lambda^{(u)}(F) \cap \sigma$. On the other hand, after flipping F , the following satisfied parity checks will become unsatisfied $\Lambda^{(u)}(F) \setminus \sigma$.

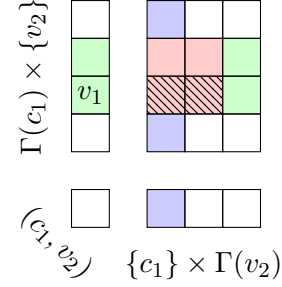
The change in the syndrome is thus

$$|\Lambda^{(u)}(F) \cap \sigma| - |\Lambda^{(u)}(F) \setminus \sigma|. \quad (7)$$

The set F can be used to decrease the syndrome if and only if the above quantity is positive.

To illustrate, we use the figure below. The parity checks lie along the line $\{v_1\} \times C_2$ corresponding to syndromes are cross hatched. The set F is a candidate set within the support of (c_1, v_2) and the corresponding qubits are colored. The green and blue squares in the support of (c_1, v_2) are colored green and blue to depict F_V and F_C respectively. Parity checks in the multi-neighborhood (in red) are flipped

twice. Parity checks in the unique neighborhood (in green/blue) are flipped once.



Suppose we restrict our attention to Z stabilizers whose local view contains UNSAT. If the syndrome σ is supported on the line $\{v_1\} \times C_2$, qubits that are themselves not on the line will never be flipped by SSF.

Claim 3. *Let $(c_1, v_2) \in C_1 \times V_2$ be a generator whose local view overlaps UNSAT non-trivially. Suppose $F \subseteq \text{supp}(c_1, v_2)$ but $F \cap \{v_1\} \times V_2 = \emptyset$. F will not be flipped by SSF.*

Proof. To evaluate the change in the syndrome, we are only concerned with the restriction of the syndrome to the local view of (c_1, v_2) . This is expressible as $\sigma \cap \Gamma(c_1) \times \Gamma(v_2) = \{v_1\} \times \sigma_C$ where σ_C is supported on $\Gamma(v_2)$.

Recall that we can write $\Lambda^{(u)}(F)$ as a disjoint union

$$F_V \times F_C^c \sqcup F_V^c \times F_C. \quad (8)$$

Therefore, we can write $\Lambda^{(u)}(F) \setminus \sigma$ in terms of these two portions separately. Let $|F_V \setminus \{v_1\}| = a$ and $|F_C \setminus \sigma_C| = b$ for the sake of readability. The quantity a expresses the number of VV qubits in the support of (c_1, v_2) that are flipped that are *not* along the line $\{v_1\} \times V_2$. The quantity b represents CC qubits *not* adjacent to the unsatisfied parity checks.

We first consider the negative contribution to the change in the syndrome, $|\Lambda^{(u)}(F) \setminus \sigma|$. As σ is only supported along $\{v_1\} \times \Gamma(v_2)$, the first portion $|F_V \times F_C^c \setminus \sigma|$ can be expressed as

$$\begin{aligned} & |(F_V \setminus \{v_1\}) \times F_C^c \setminus \sigma_C| \\ &= |F_V \setminus \{v_1\}| \cdot ((\Delta_V - |\sigma_C|) - |F_C \setminus \sigma_C|) \\ &= a[(\Delta_V - |\sigma_C|) - b]. \end{aligned} \quad (9)$$

The second portion is $|F_V^c \times F_C \setminus \sigma|$, which is

$$\begin{aligned} & |F_V^c \setminus \{v_1\} \times (F_C \setminus \sigma_C)| \\ & = ((\Delta_C - 1) - |F_V \setminus \{v_1\}|) \cdot |F_C \setminus \sigma_C| \\ & = [\Delta_C - 1 - a] \cdot b. \end{aligned} \quad (10)$$

Together, $|\Lambda^{(u)}(F) \setminus \sigma|$ is the sum of the contributions from Eq. (9) and Eq. (10):

$$\begin{aligned} & (\Delta_V - |\sigma_C|)a + (\Delta_C - 1)b - 2ab \quad (11) \\ & = (\Delta_V - |\sigma_C \cup F_C|)a + (\Delta_C - |F_V \cup \{v_1\}|)b. \end{aligned} \quad (12)$$

Next, we consider the positive contribution to the change in the syndrome, $|\sigma \setminus \Lambda^{(u)}(F)|$

$$(F_V \cap \{v_1\}) \times (\sigma_C \setminus F_C^c) \sqcup (F_V^c \cap \{v_1\}) \times (\sigma_C \setminus F_C). \quad (13)$$

Observe that v_1 can either belong to either F_V or F_V^c ; it cannot belong to both. As a result, we compute the change in the syndrome case-by-case.

Case 1: $F_V \cap \{v_1\} = \{v_1\}$. Noting that $|\sigma_C \setminus F_C^c| = |\sigma_C \cap F_C|$, the change in the syndrome is

$$= |F_C| - (\Delta_V - |\sigma_C \cup F_C|)a - (\Delta_C - |F_V|)b \quad (14)$$

Observe that $|\sigma_C \cup F_C| \leq \Delta_V$ and $|F_V| \leq \Delta_C$. Therefore, Eq. (14) is clearly maximum when $a = b = 0$.

Case 2: $F_V^c \cap \{v_1\} = \{v_1\}$. The change in the syndrome is

$$|\sigma_C \setminus F_C| - (\Delta_V - |\sigma_C \cup F_C|)a - (\Delta_C - 1 - |F_V|)b. \quad (15)$$

Again, $|\sigma_C \cup F_C| \leq \Delta_V$ and $|F_V| + 1 \leq \Delta_C$. This is maximum when $a = 0$, $b = 0$ and $F_C \cap \sigma_C = \emptyset$. However, this is simply the trivial set $F = \emptyset$. Equivalently, we can let $|F_V| = \Gamma(c_1) \setminus \{v_1\}$ and $F_C \sqcup \sigma_C = \Gamma(v_2)$.

The score is normalized by the weight of F , and therefore, we pick the smallest set F that results in the largest change in the syndrome. The only valid corrections, therefore, correspond to flipping the qubit (v_1, v_2) in the support of (c_1, v_2) . \square

Claim 2 and Claim 3 together imply Lemma 1.

B PAL implementation details

We use the implementation of OSD from Roffe *et al.* [43] and we use the variant OSD-CS. For BP, we use the min-sum variant of BP and fix the maximum number of iterations to 30. This is in contrast to [43] where BP runs for a number of iterations equal to the block length and is instead along the lines of the decoder proposed by Pantelev and Kalachev [42].

To initialize BP, we estimate the LLRs as a function of the initial error rate p_{phys} . To this end, we use the following heuristic. When SSF results in a stopping failure and the stopping set is line like, we record the average number of bit errors in that line. Of course, the final decoder does not have access to the actual distribution of errors; rather, we use this heuristic to collect data and inform our choice of LLRs. We refer to the average number of errors as q_V and q_C for line-like errors in \mathcal{C} and $\tilde{\mathcal{C}}$ respectively. These are both functions of p_{phys} and need to be measured accordingly. Inferring q_V and q_C is only done once and therefore does not affect the time complexity.

C Using PAL after BP + SSF

Using a combination SSF along with other decoding algorithms has been considered in the literature. A popular approach has been to use belief propagation (BP) followed by an appropriate post-decoding algorithm such as OSD. Similarly, SSF can also be used as a low-complexity decoder to complement BP [32]. In this section, we consider applying PAL as a post decoder for BP + SSF, forming a decoder we will call BP + SSF + PAL.

Before we specify details of BP+SSF+PAL, we first note that a number of different options have been considered for BP+SSF. The implementations in [32] used a sum-product version of BP prior to running SSF. However, the implementations in [42, 43] used a min-sum version of BP prior to running SSF, which can lead to orders-of-magnitude improvement in the logical error probability.

The implementation in in [32], which uses a sum-product version of BP, stops at regular intervals to see whether SSF can correct the error. If it cannot, it

continues running BP before trying SSF again. This poses some challenges since this sum-product version of BP often does not terminate. For instance, the total syndrome weight associated with the deduced flip oscillates with the number of iterations of BP. To handle these challenges, the user specifies the maximum number of iterations of BP to try before declaring failure.

On the other hand, we observed that the min-sum version BP (similar to that in [42, 43]) did not exhibit the oscillatory behavior which was observed in the sum-product case. We therefore implement the min-sum version of BP with a fixed number of rounds prior to SSF as specified in Algorithm 5). Moreover, the logical error rates achieved when the min-sum version of BP is used are considerably lower than those in [32] with the sum-product version. Furthermore, for the range of values that we simulate for, we did not observe an error floor. We refer to Fig. 5.

Algorithm 5 BP + SSF(R, p_{phys})

Input: $R \in \mathbb{N}$ and $p_{\text{phys}} \in [0, 1]$

Output: Correction \hat{E} .

- 1: Initialize BP with LLRs equal to $\lambda_q = \log_2((1 - p_{\text{phys}})/p_{\text{phys}})$.
 - 2: **for** $1 \leq i \leq R$ **do**
 - 3: min-sum BP.
 - 4: **for** $q \in Q$ **do**
 - 5: **if** $\lambda_q > 0$ **then**
 - 6: | $\hat{E} \leftarrow \hat{E} \cup \{q\}$
 - 7: $\sigma \leftarrow \sigma(\hat{E})$
 - 8: $\hat{E} \leftarrow \text{SSF}(\sigma)$.
 - 9: **return** \hat{E}
-

In Fig. 5, we examine the impact of running PAL after this min-sum based BP+SSF decoder with (3, 4) regular codes. Using PAL after BP+SSF(R, p_{phys}), we only observe negligible improvements for this code family because the failures were not dominated by stop failures in this case. It would be interesting to look at other code families (such as codes with larger degree) and other decoders, and observe if PAL offers more significant improvements.

D Improving time costs of the SSF decoder

In this section, we discuss the cost of naïvely implementing SSF. We then demonstrate how some of these costs can be improved. For simplicity, we only present the time cost associated with decoding Z errors. The total time cost will be twice of what we present below once we include X errors.

In Algorithm 6, we present an implementation of SSF with details regarding the associated data structures.

Overview: As we explain further below, `lookup_table` is simply a table³ of size M_Z that stores `score(c, v)` for every generator $(c, v) \in C \times V$. For each generator $(c, v) \in C \times V$, we have a data structure `generator(c, v)` that is used to compute the score and store the best subset of qubits to flip in each round.

We first sort `lookup_table` to arrange generators in decreasing order of the best score. We then find the best generator, denoted (c_i, v_i) , using the `find_best()` method of `lookup_table`.

The corresponding set of qubits that maximizes the score is denoted F_i and stored in `generator(c_i, v_i)`. It is obtained by using `generator(c_i, v_i).best_flip`. After flipping F_i , we recompute scores of the generators that have changed, and reinsert them in `lookup_table`. As only a constant number of qubits F_i have been flipped, we only need reinsert a constant number of generators into `lookup_table`.

D.1 Time complexity

In this section, we discuss the time costs associated with SSF. We can form a simple model of the run time of SSF on a fixed syndrome σ_X for a quantum expander code of length N encoding K logical qubits as follows:

$$T_{\text{SSF}} \simeq T_{\text{init}} + N_{\text{rounds}} \cdot T_{\text{update_per_round}} \quad (16)$$

In words, we can split the contribution to the cost of SSF from the time to initialize the algorithm, and

³`lookup_table` is implemented with a heap. Thus “sorting” is actually done implicitly at insertion time.

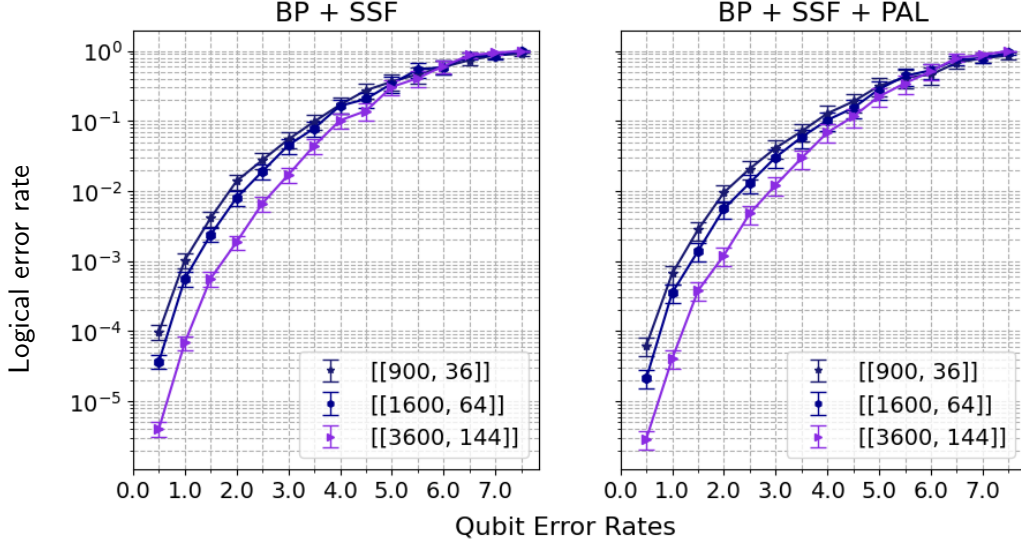


Figure 5: Comparing the change in logical error probability before and after the post-processing algorithm PAL while using BP as a pre-processing algorithm. Hypergraph product of $(3, 4)$ -biregular bipartite graphs ($\Delta_q = 8$ and $\Delta_g = 7$) are used. The error bars represent the 95% confidence intervals, i.e. ≈ 1.96 standard deviation.

then the time to perform all iterations. This can be written as a product of the number of rounds, N_{rounds} , times the time per round $T_{\text{update_per_round}}$.

1. The initialization costs T_{init} : Before each round, the algorithm needs to know the score of each generator. This then allows it to decide which generator contains the support of the correction to be applied in that round. The score of all M_Z Z -type generators are computed at the start. These scores are stored in the data structure `lookup_table` whose space and time costs we describe shortly. In our model, we suppose that the subroutine `score()` which calculates the score of a generator takes a time $T_{\text{gen-score}}$. This cycles through the power set of the support and therefore takes time $2^{\Delta_v + \Delta_c}$. This is a method for the `generator` class that we also describe below. Tallying costs, creating the table `lookup_table` takes time $N_{\text{generators}} \cdot T_{\text{gen-score}}$.

2. Number of rounds N_{rounds} : Each round of SSF strictly reduces the syndrome weight, which is initially $|\sigma_X|$. Therefore the number of rounds N_{rounds} is between zero and $|\sigma_X|$, and in our model we assume that it scales proportionally to $|\sigma_X|$, i.e., $N_{\text{rounds}} = c|\sigma_X|$ for some constant $0 < c \leq 1$.

3. Update time $T_{\text{update_per_round}}$: We can

break down $T_{\text{update_per_round}}$ as follows:

$$\begin{aligned}
 T_{\text{update_per_round}} = & \\
 & T_{\text{find_best}} \\
 & + T_{\text{update_deduced_error}} \\
 & + T_{\text{update_syndromes}} \\
 & + T_{\text{update_scores}} \cdot \quad (17)
 \end{aligned}$$

3a: $T_{\text{find_best}}$: In each iteration, we flip qubits in the support of the generator with the best score. Once we have decided to flip the corresponding set of qubits, we need to update the syndromes of the X -type parity checks.

The score for each generator is stored in the data structure `lookup_table`. The time complexity of SSF depends on the complexity of querying and updating the data structure `lookup_table`. This data structure is unspecified by the algorithm itself. It is often stated that SSF is linear time, and what is meant is that the data structure `lookup_table` only needs to be queried and updated $O(N)$ times. Regardless of how the data structure is designed, there is a fundamental trade-off between the time to find the best element using `find_best` (line 6) and the time to update elements in each iteration (lines 11-13).

We first describe the data structures

Algorithm 6 SSF(σ_X) (Formal)

Input: A syndrome $\sigma \in \mathbb{F}_2^M$.

Output: Correction \hat{E}

```
1: for every  $Z$ -type generator  $(c, v) \in C \times V$  do
2:   max-score  $\leftarrow 0$ .
3:   for  $F \in \text{supp}(c, v)$  do  $\triangleright 2^{\Delta_V + \Delta_C}$  iterations
4:     if score( $F$ ) > max-score then
5:       lookup_table( $c, v$ )  $\leftarrow$  score( $F$ )
6: lookup_table.sort()  $\triangleright O(M \cdot \log(M))$  time
7:  $\sigma_X^{(0)} \leftarrow \sigma_X$ 
8:  $\hat{E} \leftarrow \emptyset$ 
9:  $(c_i, v_i) \leftarrow \text{lookup\_table.find\_best}()$   $\triangleright O(1)$ 
   time
10:  $F_i \leftarrow \text{generator}(c_i, v_i).\text{best\_flip}()$ .
11: while score( $F_i$ ) > 0 do
12:    $\hat{E} \leftarrow \hat{E} \uplus F_i \pmod{2}$ 
13:   updated-parity-checks  $\leftarrow \emptyset$ 
14:   for Each  $X$ -type parity check  $(\nu, \zeta)$  adjacent
   to  $F_i$  do
15:      $\sigma_X^{(i+1)}[\nu, \zeta] = \sigma_X^{(i)}[\nu, \zeta] \oplus \sigma_X(F_i) \pmod{2}$ 
16:     updated-parity-checks  $\leftarrow$  updated-
   parity-checks  $\cup (\nu, \zeta)$ 
17:   for Each  $Z$ -type generator  $(c, v)$  adjacent to
   updated-parity-checks do
18:     max-score  $\leftarrow 0$ .
19:     for  $F \in \text{supp}(c, v)$  do  $\triangleright 2^{\Delta_V + \Delta_C}$  itera-
   tions
20:       if score( $F$ ) > max-score then
21:         lookup_table( $c, v$ )  $\leftarrow$  score( $F$ )
22:      $i \leftarrow i + 1$ 
23:      $(c_i, v_i) = \text{lookup\_table.find\_best}()$   $\triangleright O(1)$ 
   time
24:    $F_i \leftarrow \text{generator}(c_i, v_i).\text{best\_flip}()$ .
25: return  $\hat{E}$ .
```

lookup_table, the methods associated with it and the corresponding space and time complexity. This is summarized in Table 2.

We use a heap to build the data structure lookup_table. The time to construct the table is $\Theta(M \log M)$. The time to insert a new element is $\Theta(\log M)$ and the time to find an element is $\Theta(1)$.

3b: $T_{\text{update_deduced_error}}$: This step is simple: we update the vector \hat{E} in at most $\Delta_V + \Delta_C$ locations.

3c: $T_{\text{update_syndromes}}$: For each of the at most $\Delta_V + \Delta_C$ qubits, we need to update the syndromes of at most $\Delta_V \cdot \Delta_C$ X -type parity checks.

3d: $T_{\text{update_scores}}$: Each element of lookup_table is computed using the generator data structure which is described in Table 2.

The generator data structure stores the best flip corresponding to the generator. This requires $\Delta_V + \Delta_C$ memory, one bit per qubit in the support of the generator. As the score() method iterates through every possible flip for qubits in the support of the Z -type generator, it also stores the value of the current set of qubits in consideration and the corresponding score.

D.2 Reducing the run time to score a generator

The ideas in Section D.2 are due to Antoine Gropellier and were used in [45]. We include it here for completeness.

The most costly part of a naïve implementation of SSF is the function score_gen(). To illustrate, we include the following data from a profiler in Table 4. It is evident that speedups in score_gen would mean significant speedups overall. Gropellier's idea was to use a Gray code [46].

To compute the score for a Z generator $(c, v) \in C \times V$, we need to cycle through each subset of $\Gamma_Z(c, v)$. There are $2^{\Delta_V + \Delta_C}$ such elements which can be indexed by an integer $i \in \{1, \dots, 2^{\Delta_V + \Delta_C}\}$. To this end, we could use a lexicographic ordering on bits. The lexicographic ordering of bits is the bijection $\text{lex} : \{0, 1\}^\Delta \leftrightarrow \mathbb{Z}$, such that for $\{0, 1\}^\Delta \ni$

Method	Space cost	Time cost
<code>init</code>	$\Theta(M)$	$\Theta(M)$
<code>- score()</code>	$\Theta(1)$	$2^{\Delta_V + \Delta_C}$
<code>- insert</code>	$\Theta(1)$	$\Theta(\log(M))$
<code>find_best()</code>	$\Theta(1)$	$\Theta(1)$

Method	Space cost	Time cost
<code>init</code>	$\Theta(1)$	$\Theta(1)$
<code>score()</code>	$\Theta(1)$	$\Theta(2^{\Delta_V + \Delta_C})$
<code>best_flip()</code>	$\Theta(\Delta_V + \Delta_C)$	$\Theta(1)$

Table 2: On the left: Data structure `lookup_table`, implemented via a heap. `score()` and `insert` are subroutines of `init`. The total time for `init` is $\Theta[(2^{\Delta_V + \Delta_C} + \log(M))M]$. On the right: Data structure `generator` ($c, v \in C \times V$).

$\mathbf{x} = (x_1, \dots, x_\Delta)$:

$$(x_1, x_2, \dots, x_\Delta) \leftrightarrow 2^{\Delta-1}x_1 + \dots + 2x_{\Delta-1} + x_\Delta.$$

The obvious way to compute the score might be to use an enumeration algorithm: for $0 \leq x \leq 2^{\Delta_V}$ and $0 \leq y \leq 2^{\Delta_C}$. The local view $N(c, v)$ is the matrix of syndromes of parity checks adjacent to (c, v) , i.e.

$$N(c, v) = \begin{pmatrix} \sigma(\nu_1, \zeta_1) & \cdots & \sigma(\nu_1, \zeta_{\Delta_V}) \\ \vdots & & \vdots \\ \sigma(\nu_{\Delta_C}, \zeta_1) & \cdots & \sigma(\nu_{\Delta_C}, \zeta_{\Delta_V}) \end{pmatrix} \quad (18)$$

`score` is a function of the difference in syndromes within this local view. If we let $\mathbf{lex}(x)$ and $\mathbf{lex}(y)$, the change in the syndrome by flipping x and y is represented as

$$\mathbf{lex}(x) \cdot N(c, v) \cdot \mathbf{lex}(y) - N(c, v). \quad (19)$$

However, this obvious ordering is wasteful as it performs computations multiple times. For instance, suppose we have computed the difference in syndrome for some x and y . If we proceed in lexicographic order, the next computation would be

$$\mathbf{lex}(x) \cdot N(c, v) \cdot \mathbf{lex}(y + 1). \quad (20)$$

First, observe that $\mathbf{lex}(x) \cdot N(c, v)$ is fixed and need not be recomputed. We need only keep track of the *change* in the score. However, the trouble is that $\mathbf{lex}(y)$ and $\mathbf{lex}(y + 1)$ could differ on many locations, i.e. the Hamming weight between the two can be quite large. Although this sounds trivial, this actually leads to many redundant computations. It would be useful if $\mathbf{lex}(y)$ and $\mathbf{lex}(y + 1)$ differed in only one location as this means that only a single element of $\mathbf{lex}(x) \cdot N(c, v)$ changes. The map \mathbf{lex} by itself does not possess this property.

A Gray code is a total order on binary strings that is different from the lexicographic order. It allows

x	$\mathbf{lex}(x)$	$\mathbf{gray}(x)$
0	00	00
1	01	01
2	10	11
3	11	10

Table 3: An example of a Gray code mapping as compared to lexicographic ordering for $x \in \{0, \dots, 3\}$. Successive integers only differ in one location in the Gray code mapping.

for a different mapping from bits to integers such that only a single element changes between rounds. As an example, we contrast the gray code on 2 bits below in Table 3.

This leads to a savings in the time spent on computing `score`. We include an illustrative table below for the (3, 4) regular codes below in Table 4. For the $[[10000, 400]]$ code, there is approximately a 10 \times speedup. Before this optimization, computing the scores in each round is roughly 90% of the total run time. It drops to 55% after using the Gray code.

D.3 Reducing the number of calls of the score subroutine

The naïve algorithm is computing the `score` for generators that *certainly* cannot be the best. In particular, we can ignore a generator if it is not adjacent to an unsatisfied X -type parity check as these generators cannot possibly reduce the score. Table 5 demonstrates the performance benefits by using this observation.

For each generator, computing the score takes $\Theta(2^{\Delta_V + \Delta_C})$ time. This can be reduced if we can restrict the weight of the flip F to size w . In this case, the time complexity would scale in proportion to $\binom{\Delta_V + \Delta_C}{w}$ which can be significantly less than

Algorithm	number score gen calls	Avg. run time per call (s)	Avg. run time for all calls (s)	Avg. run time per sample (s)
SSF ₀	1988	2.1×10^{-5}	4.2×10^{-2}	4.6×10^{-2}
SSF ₁	1990	1.7×10^{-6}	3.4×10^{-3}	6.1×10^{-3}

Table 4: Comparison of the costs and error correction performance of an unoptimized implementation SSF₀ and an implementation of SSF, SSF₁, with the Gray code for length 10000 HGP code with $p = 0.01$ error rate.

Algorithm	number score gen calls	Avg. run time (s)
SSF ₁	1988	6.1×10^{-3}
SSF ₂	1369	4.4×10^{-3}

Table 5: Comparison of the costs and error correction performance of SSF₁ that uses the Gray code and an optimized implementation of SSF, SSF₂, that avoids generators not adjacent to unsatisfied parity checks for a $[[10000, 400]]$ code with $\Delta_V = 3, \Delta_C = 4$ and $p = 0.01$ error rate.

$2^{\Delta_V + \Delta_C}$. Furthermore, if *most* flips had low weight, it could significantly improve the time spent computing the score. Theoretical results [26–28] cannot guide us here. They only prove that in each iteration of SSF, there exists a generator within whose support we can find *some* set of qubits to reduce the error weight.

Consider a quantum expander code generated from the product of $(3, 4)$ -biregular graphs G . For a generator $(c, v) \in C \times V$, let $N(c, v)$ denote the local view of the Z -type generator and $|N(c, v)|$ denote the weight of the generator, i.e. the number of unsatisfied parity checks in the local view.

For $i \in \{1, \dots, 4\}$, let $r_{ba}(i)$ denote the row weight of the i^{th} row of $N(c, v)$. Similarly, for $j \in \{1, \dots, 3\}$, let $c_{ba}(j)$ denote the column weight of the j^{th} row of $N(c, v)$. We call this the **Waterfall** algorithm.

The following claim shows that the algorithm works as expected.

Claim 4. *Let $G, N(c, v), r_{ba}$ and c_{ba} be defined as above. If $|N(c, v)| \leq 3$, it suffices to run Algorithm Waterfall.*

Proof. When the local view satisfies $|N(c, v)| \leq 3$, there are very few cases to test owing to equivalence up to row and column permutations. This means

Algorithm 7 Waterfall

```

1: if  $\exists i \in \{1, \dots, 4\}$  such that  $r_{ba}(i) \geq 2$  then
2:    $\text{score}(c, v) \leftarrow |3 - 2r_{ba}(i)|$ 
3:    $F^* \leftarrow \{i\}$ 
4: else if  $\exists j \in \{1, 2, 3\}$  such that  $c_{ba}(j) = 3$  then
5:    $\text{score}(c, v) \leftarrow |4 - 2c_{ba}(j)|$ 
6:    $F^* \leftarrow \{j\}$ 
7: else if  $\exists j \in \{1, 2, 3\}$  such that  $c_{ba}(j) = 2 \wedge$ 
    $r_{ba}(i) = 1$  then
8:    $\text{score}(c, v) = 0.5$ 
9:    $F^* \leftarrow \{i, j\}$ 
10: else
11:    $\text{score}(c, v) \leftarrow 0$ 
12:    $F^* \leftarrow \emptyset$ 

```

that *locally*, i.e. from the point-of-view of a generator $(c, v) \in C \times V$, the number of rows and columns flipped is only a function of the weight of the local view $N(c, v)$. Each of these scenarios is listed below.

Case 1: $|N(c, v)| = 1$.

In this case, there is no valid flip. To prove this, it is sufficient to assume that the $(1, 1)$ entry of the matrix $N(c, v)$ is unsatisfied.

Case 2: $|N(c, v)| = 2$.

If the two unsatisfied parity checks are not in the same row, then, there is no valid flip. To prove this, it is sufficient to consider the following: assume that the $(1, 1)$ entry is unsatisfied and

- $(2, 1)$ entry is unsatisfied. This shows that if two unsatisfied parity checks are adjacent to the same CC qubit, then no flip exists.
- $(2, 2)$ entry is unsatisfied. This shows that if two unsatisfied parity checks are not adjacent to the same VV or CC qubit, then no flip exists.

Algorithm	Calls to <code>score_gen</code>	Calls to <code>Waterfall</code>	Time (s)
<code>SSF₂</code>	5,508	0	9.8×10^{-3}
<code>SSF₃</code>	220	5,268	7.0×10^{-3}

Table 6: Number of average calls to `score_gen` before and after `Waterfall` for a code with 10000 physical qubits (3, 4) codes with $p = 0.01$. `SSF2` merely ignores generators not adjacent to unsatisfied parity checks whereas `SSF3` utilizes `Waterfall`.

If they are in the same row $i \in \{1, \dots, 4\}$, then we flip that row.

Case 3: $|N(c, v)| = 3$.

If the three unsatisfied parity checks are such that no two of them are in the same row or column, then there is no valid flip. There is only one case to consider: let the (1, 1), (2, 2) and (3, 3) entries of $N(c, v)$ be unsatisfied.

There are many ways we can find a valid flip.

1. If there are two or more unsatisfied parity checks in a single row $i \in \{1, \dots, 4\}$, then flip row i .
2. If there are two unsatisfied parity checks in one column $j \in \{1, 2, 3\}$ and a row i such that the (i, j_i) entry is unsatisfied where $j_i \neq j$, then we flip both row i and column j .

□

The time improvements offered by `Waterfall` are shown in Table 6. We find a modest improvement in the total time required.